Int. J. Solids Structures, 1970, Vol. 6, pp. 975 to 993. Pergamon Press. Printed in Great Britain

DEFORMATION OF A SUPPORTED SHORT CYLINDRICAL SHELL OF ALUMINUM ALLOY UNDER INTERNAL PRESSURE

Y. OHASHI and N. KAMIYA

Department of Mechanical Engineering, Faculty of Engineering, Nagoya University, Nagoya, Japan

Abstract—In order to analyze the deformation due to internal pressure of thin cylindrical shells of materials having nonlinear stress–strain relations, fundamental equations were derived by using Kirchhoff's hypothesis and introducing a parameter showing the effect of compressibility of the material. The equations were applied to a supported short cylindrical shell of aluminum alloy under internal pressure. In order to investigate the validity of the assumptions, the analytical results were compared with experimental results.

The analytical results of the axial strain components on the outer and inner surfaces are remarkably different from each other. The complicated variation of the distribution of axial strain on the inner surface with increase of pressure is attributed to the nonlinearity of the deformation, and such a trend was verified clearly by the corresponding experiment.

NOTATION

$a, 2h, 2l$	dimensions of circular cylindrical shell (Fig. 1)
a_0, a_1, a_2, a_3	material constants [equation (26)]
$a_{ij}, b_i\ (i,j = 1,2,3)$	matrix elements defined by equation (29) (Appendix II)
c	parameter characterizing material compressibility
e_x, e_θ	unit elongations of middle surface
$\bar{e}$	effective strain
$\bar{e}_{eq}$	volumetric mean of $\bar{e}$
$E_1, \beta, \omega_1, \omega_0$	variable parameters defined in equation (22)
I_1, I_2, I_3	symbols defined by equation (25)
M_x, M_θ	bending moments per unit length of middle surface
p	internal pressure
Q_x	shearing force per unit length of middle surface
$s = -\mathrm{d}w/\mathrm{d}x$	gradient of radial displacement [equation (19)]
T_x, T_θ	membrane forces per unit length of middle surface
u, w	displacements
x, θ, z, or $x_i\ (i = 1,2,3)$	orthogonal coordinate system (Fig. 1)
α	coefficient of volumetric strain
α_x, α_θ	changes in curvature of middle surface
$\delta_{ij}\ (i,j = 1,2,3)$	Kronecker's symbol
ε	mean normal strain
$\varepsilon_x, \varepsilon_\theta$ or $\varepsilon_{ij}\ (i,j = 1,2,3)$	strain components
σ	mean normal stress
$\bar{\sigma}$	effective stress
$\sigma_x, \sigma_\theta, \tau_{xz}, \tau_{x\theta}, \tau_{z\theta}$ or $\sigma_{ij}\ (i,j = 1,2,3)$	stress components

1. INTRODUCTION

DEFORMATION analyses of cylindrical shells of finite length subjected to internal pressure have been carried out in detail in elasticity [1]. In plasticity however, only limit analysis has been applied for such problems [2, 3]. On the other hand, though limit analysis may be

available for materials having a discrete yield point such as mild steel, it cannot be applied in a sufficiently wide range of deformation for a cylindrical shell of a material with a non-linear stress–strain relation.

Therefore, in the present paper, fundamental equations are derived to analyze the axisymmetric deformation of a cylindrical shell under internal pressure for materials having non-linear stress–strain relations. In the analysis, Kirchhoff's hypothesis is used under the assumption that the shell is thin. Moreover, Hencky's equation is used for the plastic stress–strain relation, and, for considering the effect of compressibility of the material, a parameter related to the mean value of effective strain over the whole region subjected to the assigned pressure is introduced. The non-linear stress–strain relation of the material obtained by a calibration test is approximated by a polynomial of four terms.

Since the above mentioned assumptions are approximations to simplify the analysis, the fundamental equations derived from them must be discussed with respect to their applicable ranges by comparing them with the corresponding experimental results. For this purpose the equations are applied to the deformation of a supported short cylinder of aluminum alloy subjected to internal pressure.

2. STRESS–STRAIN RELATION OF COMPRESSIBLE MATERIALS [4, 5]

In restricting the range of deformation to be small, Hencky's relation may be assumed to hold between the components of the stress and strain deviators,

$$\sigma_{ij}-\sigma\delta_{ij}=\frac{2\bar{\sigma}}{3\bar{e}}(\varepsilon_{ij}-\varepsilon\delta_{ij}), \qquad (i,j=1,2,3) \tag{1}$$

where

$$\sigma=\tfrac{1}{3}\sigma_{ii}, \qquad \varepsilon=\tfrac{1}{3}\varepsilon_{ii},$$
$$\bar{\sigma}=\sqrt{\tfrac{3}{2}[(\sigma_{ij}-\sigma\delta_{ij})(\sigma_{ij}-\sigma\delta_{ij})]}, \qquad \bar{e}=\sqrt{\tfrac{2}{3}[(\varepsilon_{ij}-\varepsilon\delta_{ij})(\varepsilon_{ij}-\varepsilon\delta_{ij})]}.$$

It is also assumed that the following relation holds between the mean normal stress and strain

$$\varepsilon=\alpha\sigma, \tag{2}$$

where the coefficient of volumetric strain α is constant.

Substituting equation (2) into equation (1), the stress components are obtained as follows;

$$\sigma_{ij}=A(\bar{e})\varepsilon_{ij}+B(\bar{e})\varepsilon\delta_{ij}, \tag{3}$$

where

$$A(\bar{e})=2\bar{\sigma}/3\bar{e}, \qquad B(\bar{e})=\frac{1}{\alpha}(1-2\bar{\sigma}\alpha/3\bar{e}),$$

or, setting now

$$c(\bar{e})=2\bar{\sigma}\alpha/3\bar{e}, \tag{4}$$

they are represented in the following form;

$$\sigma_{ij} = A(\bar{e})\left[\varepsilon_{ij}+\frac{1-c(\bar{e})}{c(\bar{e})}\varepsilon\delta_{ij}\right]. \tag{5}$$

The Kirchhoff hypotheses, also known as the Kirchhoff–Love hypotheses, are frequently applied to the theoretical analysis of the deformation of thin plates and shells. By employing the hypotheses that the transverse normal stress can be neglected ($\sigma_{33} = 0$) in comparison with the other stress components (the x_1 and x_2 coordinate curves lie on the middle surface of the plate or shell and x_3 is perpendicular to it), the transverse normal strain, the volumetric strain and the effective strain respectively, are formally expressed by using equation (5) as follows,

$$\varepsilon_{33} = \frac{c(\bar{e})-1}{2c(\bar{e})+1}(\varepsilon_{11}+\varepsilon_{22}), \qquad 3\varepsilon = \frac{3c(\bar{e})}{2c(\bar{e})+1}(\varepsilon_{11}+\varepsilon_{22}), \tag{6}$$

$$\bar{e} = \frac{2}{\sqrt{3}}\left[\frac{1+c(\bar{e})+c^2(\bar{e})}{(1+2c(\bar{e}))^2}(\varepsilon_{11}+\varepsilon_{22})^2-\varepsilon_{11}\varepsilon_{22}+\varepsilon_{12}^2+\varepsilon_{23}^2+\varepsilon_{31}^2\right]. \tag{7}$$

Substituting equations (6), equation (5) becomes

$$\sigma_{11} = A(\bar{e})\left[\frac{2+c(\bar{e})}{1+2c(\bar{e})}\varepsilon_{11}+\frac{1-c(\bar{e})}{1+2c(\bar{e})}\varepsilon_{22}\right], \qquad \sigma_{22} = A(\bar{e})\left[\frac{2+c(\bar{e})}{1+2c(\bar{e})}\varepsilon_{22}+\frac{1-c(\bar{e})}{1+2c(\bar{e})}\varepsilon_{11}\right],$$
$$\sigma_{33} = 0, \qquad \sigma = A(\bar{e})\varepsilon_{12}, \qquad \sigma_{23} = A(\bar{e})\varepsilon_{23}, \qquad \sigma_{31} = A(\bar{e})\varepsilon_{31}. \tag{8}$$

The value of $c(\bar{e})$ is defined by equation (4) and can be determined experimentally, for example, by a uniaxial tension test (Fig. 7). It is apparent from Fig. 7 that $c(\bar{e})$ decreases with increase of $\bar{e}$. Since the first term in the right hand side of equation (7) contains $c(\bar{e})$ dependent on $\bar{e}$, equation (7) does not define $\bar{e}$ explicitly. On the other hand, the result in Fig. 7 and the definition (4) indicate that the value of $c(\bar{e})$ is small compared with unity and that it vanishes for an incompressible material.

Since the influence of a small variation of $c(\bar{e})$ on the deformation does not seem to be severe, for convenience of analysis, a constant value defined in the following, corresponding to each external load, for the value of $c(\bar{e})$ entered in equations (7) is used. The average value of $\bar{e}$ over the deformed body, $\bar{e}_{eq} = \int \bar{e}\,dv/\int dv$, is considered to represent the deformed state under each external load. The value of $c(\bar{e})$ obtained from Fig. 7 by using $\bar{e}_{eq}$, $c(\bar{e} = \bar{e}_{eq})$, may be considered as a constant corresponding to the prescribed load. Hereafter it is written as c instead of $c(\bar{e})$.

Since the above approximation is, however, based on the average distribution of $\bar{e}$ over the entire volume, it is noted that it does not take account completely of the local effect of a steep change in strain distribution and concentrated strain.

The considerations described above were applied to the analyses of the deformation of circular plates under lateral load and the analytical results agreed fairly well with the corresponding experimental ones [4, 5]. Since the deformation of thin walled circular cylindrical shells subjected to internal pressure may also be treated as a plane stress problem, in this paper, it is analyzed in a similar manner to the previous papers [4, 5].

3. FUNDAMENTAL EQUATIONS

As shown in Fig. 1, a coordinate system x, θ, z is considered at the center on the middle layer of the cylindrical shell under internal pressure. The shell is assumed so thin that a state of plane stress may be considered,

$$\sigma_z = \tau_{xz} = 0.$$

The stresses $\tau_{x\theta}$ and $\tau_{z\theta}$ vanish on account of geometrical symmetry. The remaining stresses are expressed by using equations (8) as follows:

$$\sigma_x = \frac{2\bar{\sigma}}{3\bar{e}}\left[\frac{2+c}{1+2c}\varepsilon_x + \frac{1+c}{1+2c}\varepsilon_\theta\right], \quad \sigma_\theta = \frac{2\bar{\sigma}}{3\bar{e}}\left[\frac{2+c}{1+2c}\varepsilon_\theta + \frac{1-c}{1+2c}\varepsilon_x\right]. \tag{9}$$

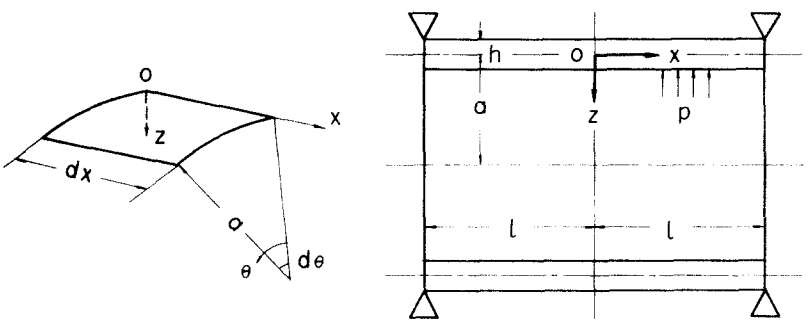

FIG. 1. Coordinate system. Cylindrical shell under internal pressure.

By using the components of bending moment M_x, M_θ, membrane force T_x, T_θ and shearing force Q_x, the equilibrium conditions of the shell for small deformations are expressed as

$$\mathrm{d}T_x/\mathrm{d}x = 0, \tag{10}$$

$$\mathrm{d}Q_x/\mathrm{d}x + T_\theta/a = p, \tag{11}$$

$$\mathrm{d}M_x/\mathrm{d}x - Q_x = 0. \tag{12}$$

From the components of unit elongation e_x, e_θ and the change of curvature α_x of the middle surface of the shell, with another assumption of Kirchhoff, the components of strain are expressed as follows:

$$\varepsilon_x = e_x + z\alpha_x, \qquad \varepsilon_\theta = e_\theta. \tag{13}$$

The change of curvature in the circumferential direction may be neglected in the small deformation theory:

$$\alpha_\theta = 0. \tag{14}$$

With the use of the radial displacement w and the axial displacement u, the values e_x, e_θ and α_x are expressed as [1]

$$e_x = \mathrm{d}u/\mathrm{d}x, \qquad e_\theta = -w/a, \qquad \alpha_x = -\mathrm{d}^2w/\mathrm{d}x^2. \tag{15}$$

Eliminating w from equation (15), the following relation is obtained:

$$d^2e_\theta/dx^2 = \alpha_x/a. \tag{16}$$

Since the shear stress τ_{xz} is usually neglected, and the shear force Q_x cannot be expressed as an integration of the stress through the thickness, the equation

$$d^2M_x/dx^2 = p - T_\theta/a, \tag{17}$$

which is obtained by eliminating Q_x from equations (11) and (12), is used for the analysis. However, in that case, it is necessary to consider a system of second order differential equations, by differentiating equation (10) as follows:

$$d^2T_x/dx^2 = 0, \tag{18}$$

to solve the fundamental equations numerically. However, as shown later, since the components of the bending moment and the membrane force contained in equations (17) and (18) are expressed by the components of strain, it will be very cumbersome to differentiate each of the components twice with respect to x. Moreover, the numerical solution of a system of second order differential equations is much more difficult to obtain than that of a system of first order equations. The following method is, therefore, intended to avoid such a difficulty. In the method, the shear force Q_x is considered as a parameter related to x, and another parameter s is introduced as follows:

$$s = -dw/dx. \tag{19}$$

By using the parameter s, the compatibility condition of strain (16) is divided into two differential equations of first order

$$de_\theta/dx = s/a, \tag{20}$$

$$ds/dx = \alpha_x. \tag{21}$$

Consequently, the system of fundamental equations consists of five equations, (10)–(12), (20) and (21), and these are all first order differential equations with respect to x.

As in the previous paper [5], the components of strain e_x, e_θ and those of change of curvature α_x, α_θ are transformed by using the parameters E_1, β, ω_1 and ω_0 as follows:

$$\left.\begin{matrix} e_x \\ e_\theta \end{matrix}\right\} = \frac{2E_1}{\sqrt{3}}[\cos(\omega_1 \mp \pi/3) + c\cos\omega_1],$$
$$\left.\begin{matrix} \alpha_x \\ \alpha_\theta \end{matrix}\right\} = \frac{2\beta E_1}{\sqrt{3}h}[\cos(\omega_0 \mp \pi/3) + c\cos\omega_0]. \tag{22}$$

In the above relations, as α_θ may be considered as zero identically for small deformations, it follows that:

$$\cos(\omega_0 + \pi/3) + c\cos\omega_0 = 0. \tag{23}$$

Therefore, the value of ω_0 may be found as a constant for the assigned pressure, because the value of c may be obtained as a constant for each assigned pressure. Then, from equation (14), e_x, e_θ and α_x may be considered as functions of E_1, β and ω_1.

As usual, the components of the bending moment and the membrane force are obtained by integrating through the thickness the components of stress and its moment. By using equations (9) and (22), these values are expressed as follows;

$$\left.\begin{matrix} T_x \\ T_\theta \end{matrix}\right\} = \pm\tfrac{4}{3}E_1 h[\sin(\omega_1 \pm \pi/3)I_1 + \beta \sin(\omega_0 \pm \pi/3)I_2],$$
$$\left.\begin{matrix} M_x \\ M_\theta \end{matrix}\right\} = \pm\tfrac{4}{3}E_1 h^2[\sin(\omega_1 \pm \pi/3)I_2 + \beta \sin(\omega_0 \pm \pi/3)I_3] \tag{24}$$

where

$$I_1 = \frac{1}{h}\int_{-h}^{h} (\bar{\sigma}/\bar{e})\,\mathrm{d}z, \qquad I_2 = \frac{1}{h^2}\int_{-h}^{h} (\bar{\sigma}/\bar{e})z\,\mathrm{d}z, \qquad I_3 = \frac{1}{h^3}\int_{-h}^{h} (\bar{\sigma}/\bar{e})z^2\,\mathrm{d}z. \tag{25}$$

The non-linear stress–strain relation of the material obtained from calibration test is approximated by the following polynomial:

$$\sigma = a_0\bar{e} + a_1\bar{e}^2 + a_2\bar{e}^3 + a_3\bar{e}^5. \tag{26}$$

The concrete form of equation (24) is expressed in detail in Appendix I. By integrating equation (10), the following relation is obtained;

$$T_x = \text{const.}, \tag{27}$$

where the value of the integration constant is to be obtained from the boundary conditions. Then, the three parameters E_1, β and ω_1 are not independent of each other and the functional relation may be selected as follows;

$$\omega_1 = \omega_1(E_1, \beta), \tag{28}$$

where the concrete form of the relation, which is to be found by solving the transcendental equation (27), is difficult to express formally. Then, $E_1(x)$ and $\beta(x)$ may be considered as the independent parameters which are variable with respect to x.

By substituting equations (22) and (24) into equations (10), (12) and (20), the system of fundamental differential equations is expressed as

$$\begin{pmatrix} a_{11} & a_{12} & a_{13} \\ a_{21} & a_{22} & a_{23} \\ a_{31} & a_{32} & a_{33} \end{pmatrix} \begin{pmatrix} \mathrm{d}E_1/\mathrm{d}x \\ \mathrm{d}\beta/\mathrm{d}x \\ \mathrm{d}\omega_1/\mathrm{d}x \end{pmatrix} = \begin{pmatrix} b_1 \\ b_2 \\ b_3 \end{pmatrix}, \tag{29}$$

where the expressions for the elements of the square matrix (a_{ij}) and those of the column matrix (b_i) on the right hand side are rather complicated and are shown in Appendix II.

As the value of c contained in equation (4) depends on the deformed state as well as the characteristics of the material, it is difficult to estimate in advance. We now employ a method used in previous papers [4, 5]. The method consists of three steps. Firstly, the fundamental equations are solved for the assigned value of p under the assumption of $c = 0$. From the result, the distribution of effective strain is found over the shell, and its volumetric mean value $\bar{e}_{eq}$ is estimated. By assuming that $\bar{e}_{eq}$ represents the state of the whole shell, the corresponding value of c for the assigned value of p is obtained from the relation between

c and $\bar{e}$ of the material obtained by calibration test under uniaxial stress state. By repeating the numerical integration with the use of c just obtained, the deformation analysis of the shell may be completed.

4. NUMERICAL EVALUATION AND ITS RESULTS

The values of the constants a_0, a_1, a_2 and a_3 contained in the polynomial stress–strain relation (26) were determined by calibration tests using uniaxial tension specimens from a cylindrical shell of aluminum alloy in the manner discussed in Section 5(a), and they have the following values:

$$a_0 = 1{\cdot}139 \times 10^4, \qquad a_1 = -2{\cdot}877 \times 10^6, \qquad a_2 = 2{\cdot}784 \times 10^8$$

$$a_3 = -9{\cdot}541 \times 10^{11} \quad (\mathrm{kg/mm^2}).$$

The fundamental equations were applied for a supported short cylindrical shell with axially movable ends having ratios $a/h = 40$ and $l/a = 0{\cdot}5$. The boundary conditions are expressed as follows:

$$M_x = T_x = w = 0 \quad \text{at} \quad x = \pm l. \tag{30}$$

The results of the evaluation are shown in Figs. 2–6 and Table 1. Figure 3 shows the components of the bending moment M_x/h^2 and M_θ/h^2, where the location of the maximum value lies within the range $0{\cdot}6 \leq x/l \leq 0{\cdot}8$. In the case of linear elasticity, when the distributions vary proportionally with pressure, the location of the maximum value does not move with pressure. However, according to the solution obtained here, the maximum moves towards the center with increase of pressure. Moreover, the maximum value of M_x/h^2 decreases with increasing pressure for pressures higher than 70 kg/cm^2, while that of M_θ/h^2 increases with increase of pressure. These trends are quite different from the corresponding elastic solution.

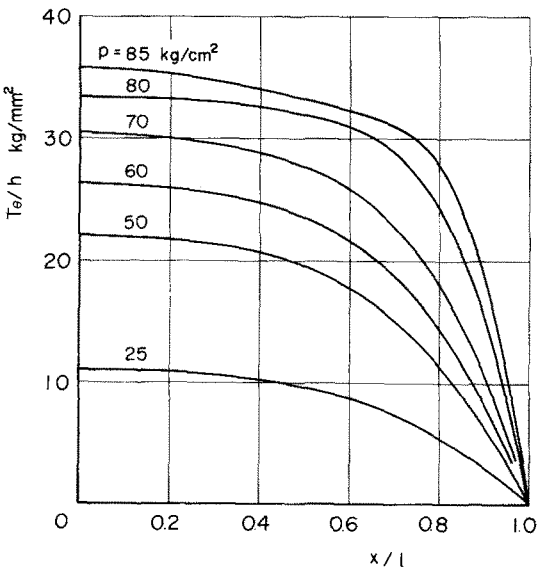

FIG. 2. Distributions of circumferential component of membrane force.

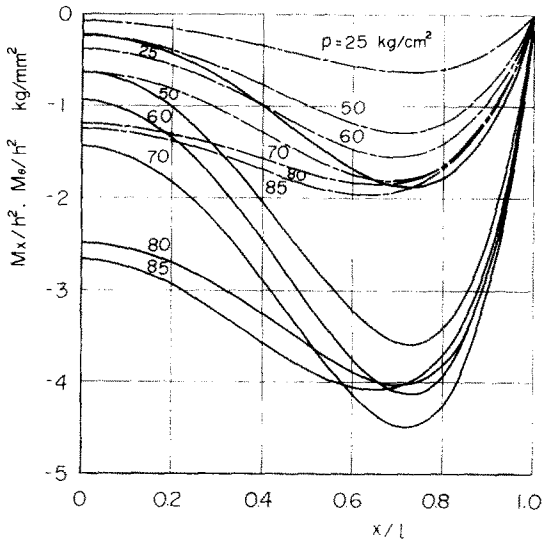

FIG. 3. Distributions of axial (solid line) and circumferential (chain line) components of bending moment.

Though the values of M_x/h^2 and M_θ/h^2 are less than that of T_θ/h, since the ratio of maximum value of $|M_x/h^2|$ to that of $|T_\theta/h|$ is about 0·16 for $p = 60\,\text{kg/cm}^2$ for example, the former values are not negligible in comparison with the latter as in the membrane theory.

Figure 4 shows the radial and axial displacements of the cylindrical shell. In linear elasticity, two different distribution modes of w have been recognized according to a parameter $\sqrt[4]{[3(1-\nu^2)]}\sqrt{(l^2/2ah)}$, which contains the Poisson's ratio ν and the geometry of

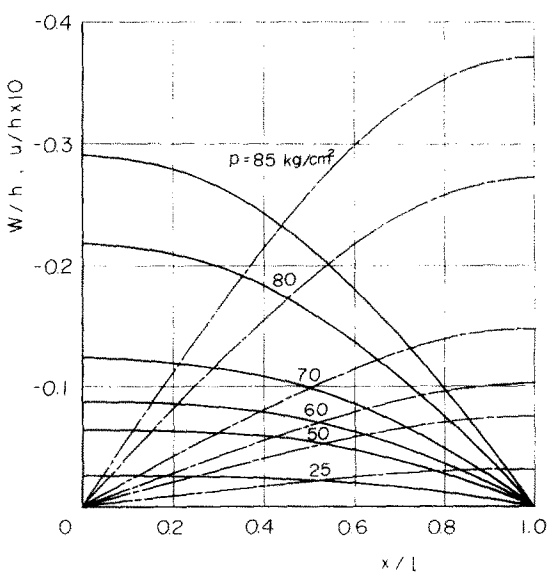

FIG. 4. Distributions of radial (solid line) and axial (chain line) displacements.

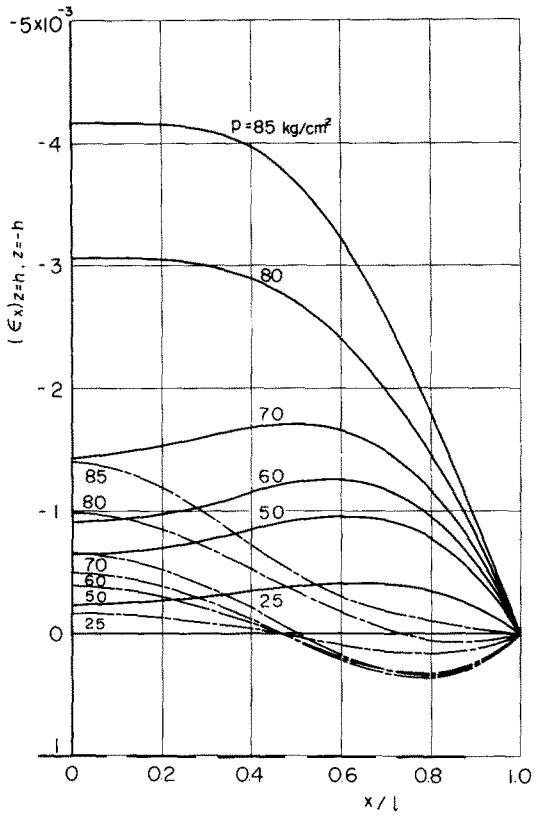

FIG. 5. Distributions of axial strain components on inner (solid line) and outer (chain line) surfaces.

the cylinder [1]. That is, a mode in which the maximum value of w appears at the center $x = 0$ corresponds to the shorter cylinder, and another mode in which the maximum value of w appears not at $x = 0$ but somewhere distant from the center corresponds to the longer ones. As the ratio l^2/ah of this example belongs to the former mode in elasticity, as shown in Fig. 4, a mode corresponding to the shorter shell in elasticity was obtained also in the analysis using a non-linear stress–strain relation.

Figure 5 shows the axial strain components on the inner surface $z = h$ and the outer surface $z = -h$, where a remarkable difference can be recognized between them. Moreover, the distribution on each surface varies strikingly with increase of pressure. These effects are the consequence of bending action.

5. EXPERIMENT

5(a). *Material of specimen*

The aluminum alloy used for the specimen has the chemical components and mechanical properties shown in Table 2, and the stress–strain relation and the relation between the parameter c and the effective strain as shown in Fig. 7. The cylindrical specimen was prepared from the raw cylinder with outer diameter 270 mm and wall thickness 10 mm.

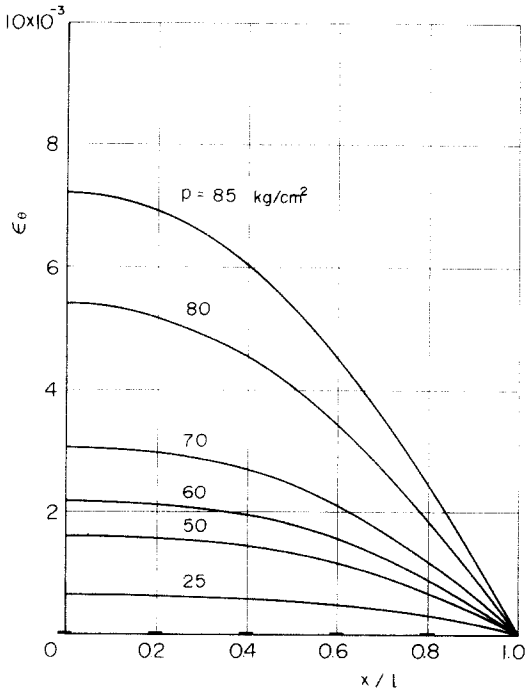

FIG. 6. Distributions of circumferential strain component.

For finding the stress–strain relation of this material, the uniaxial tension specimens as shown in Fig. 8 were cut out in the circumferential and axial directions from the raw cylinder. Moreover, as the specimen in the circumferential direction cannot be cut from the raw cylinder as it is, it was prepared by the following procedures. The arched strip with arc length of about 170 mm as shown by a fine line in Fig. 8 was cut out first. The central part of 50 mm length was fixed with a vice together with the closely fitted guards on both sides, and its ends were stretched out as shown by the dashed line. The specimen was cut from the piece obtained in that manner. The results of calibration tests performed with two specimens each in both directions are shown in Fig. 7. As shown in Fig. 7, the stress–strain relations found in the axial and circumferential directions deviated from each other within the order of 5 per cent in the plastic range. Therefore, the material may be assumed as almost

TABLE 1. VALUES OF E_1, β AT $x = 0$ AND THE PARAMETER c

p(kg/cm^2)		25	50	60	70	80	85
Incompressible	$E_{1(x=0)} \times 10^3$	0·498079	1·21890	1·66242	2·37934	4·30637	5·55145
($c = 0$)	$\beta_{(x=0)}$	0·066223	0·119073	0·138546	0·165323	0·232753	0·255879
$\bar{e}_{eq} \times 10^6$		450	1030	1380	1930	3320	4140
c		0·270	0·270	0·262	0·235	0·182	0·163
Compressible	$E_{1(x=0)} \times 10^3$	0·490412	1·21179	1·65583	2·36525	4·29263	5·75562
($c \neq 0$)	$\beta_{(x=0)}$	0·055473	0·077519	0·094713	0·125628	0·195964	0·196902

TABLE 2. CHEMICAL COMPONENTS AND MECHANICAL PROPERTIES OF MATERIAL

Chemical components (%)								
Cu	Si	Fe	Mn	Mg	Zn	Cr	Ti	Al
0·02	0·08	0·19	0·66	4·57	0·03	0·22	<0·01	*R*

Mechanical properties		
Proof stress (kg/mm²)	Tensile strength (kg/mm²)	Elongation (%)
16·1	33·9	20·3

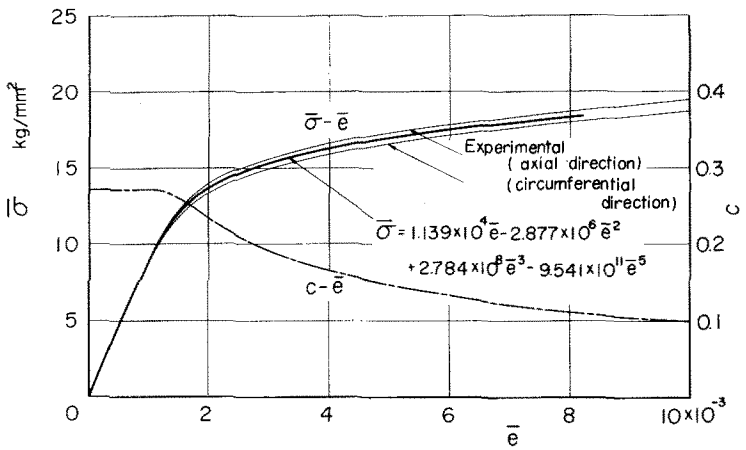

FIG. 7. Stress–strain relation and relation between the parameter c and the effective strain.

isotropic and the average relation shown by the thick curve may be substituted instead of the two fine curves. The stress–strain relation expressed by the polynomial with the above mentioned values a_0 to a_3 coincides with the averaged curve almost completely.

5(b). *Cylindrical shell specimen*

The cylindrical shell specimen with outer diameter 269 mm, thickness $2h$ = 6·5 mm and length 134 mm was prepared from the raw cylinder by fine turning of both surfaces.

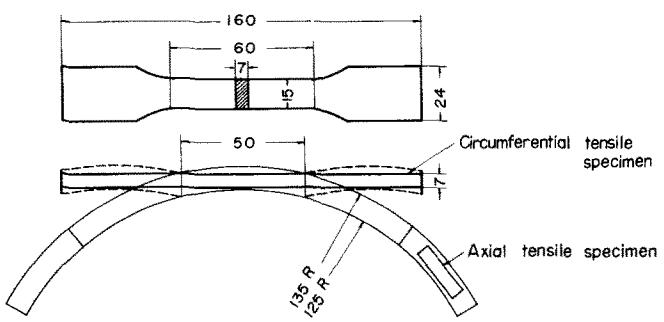

FIG. 8. Uniaxial tension specimen.

As the parts of 1·5 mm wide at both ends of the cylinder are lapped over by the supporting circle (Fig. 9), the effective length $2l$ of the specimen becomes 131 mm. Then, the specimen has the mean diameter $2a = 262{\cdot}5$ mm and the ratios $a/h = 40$ and $l/a = 0{\cdot}50$ corresponding to the values used in the above calculation.

5(c). *Experimental apparatus*

The experimental apparatus used is shown in Fig. 9, where both ends of specimen are supported with the circles inside the thick circular disks of mild steel joined together with 16 bolts. The circular disk has sufficient rigidity not to show any visible deformation under the applied pressure. The inner diameter of the supporting circle was finished as precisely as possible. To keep the distance between the two disks precisely equal to the effective length of the specimen, the central part of the bolt which is equal to the effective length was finished somewhat thicker with sharp steps at both of its ends. The cylinder was subjected to oil pressure from inside, and the pressure was measured with a Bourdon-type pressure gauge.

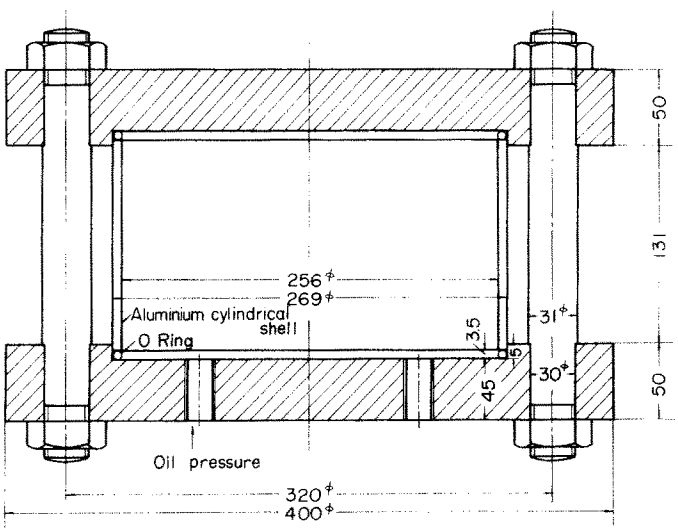

FIG. 9. Experimental apparatus.

Correct support of the specimen is most important on the apparatus. Therefore, the length of overlapped parts at both ends of the specimen with supporting circles were designed somewhat longer.

5(d). *Experimental procedure and its result*

For measuring the components of strain on both surfaces in the axial and circumferential directions, wire resistance strain gauges with gauge length 10 mm and grid width 2 mm were attached at the points corresponding to $x/l = 0$, 0·2, 0·4, 0·6 and 0·8 on both surfaces. As the strain components which are to be measured by these gauges correspond to the mean value of the distribution within 10 mm in the axial direction and within 2 mm

in the circumferential direction around the above-mentioned points, the analytical values corresponding to them are to be mean values within the ranges shown with thick line segments on the abscissa in Figs. 5 and 6.

As the value of w was extremely small, it was measured by dial indicators with minimum graduations of 0·001 mm at the location corresponding to $x/l = 0$, 0·25, 0·50 and 0·75. Although the value of w at the supported ends was supposed not to exist, it was difficult to avoid very slight clearances between the specimen and the supporting circle. Accordingly the dial indicators were arranged also there.

Figures 10–13 show the results obtained by the experiment where various small circles represent the experimental values and the solid curves show the corresponding analytical results.

6. DISCUSSION AND CONCLUSIONS

6(a). *Radial displacement*

Since the experimental values of radial displacement at the supported ends due to slight clearances are far smaller than the corresponding values at other positions of the specimen, the experimental value of w at each measuring point was determined by subtracting the value at the support from the corresponding measured values. Figure 10 shows the relation between the values determined above and the pressure. In this figure, these values agree very well with the corresponding analytical results in the range of $p \leq 65\ \text{kg/cm}^2$, and the difference between them becomes fairly large thereafter. On the other hand, according to the relation $\varepsilon_\theta = -w/a$, the radial displacement has a close relation with the value of circumferential strain component ε_θ. As shown in Fig. 13, however, the analytical and experimental values of ε_θ at each measuring point have a fairly good agreement with each other in the range of $p \geq 65\ \text{kg/cm}^2$. Accordingly the difference between results in Fig. 10 should be attributed to the experimental error in the measurement of radial displacement.

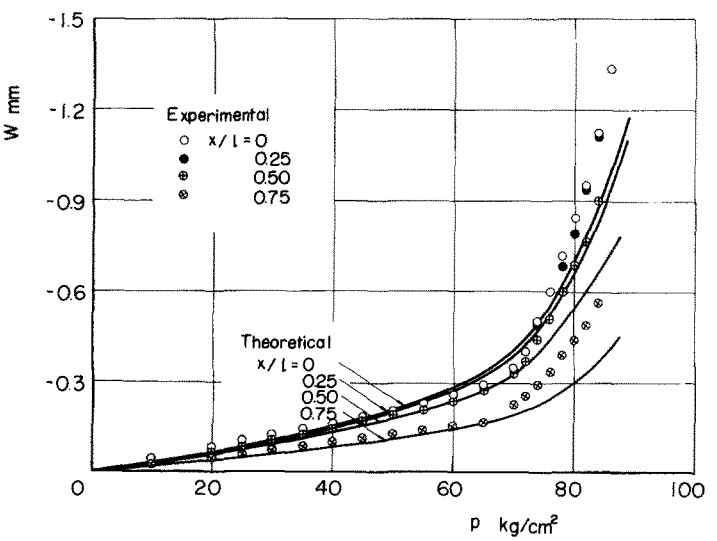

FIG. 10. Relation between radial displacement and pressure.

In the case of a circular plate under lateral load [5] made of almost the same material as the present specimen, the comparatively clear distinction between linear elastic and strain hardening plastic ranges shown in the results of calibration tests of the material could not be found in the relation between deflection and load. In the present results, however, the distinction is fairly clear in the relation between radial displacement and pressure. This may be attributed to the difference of stress distribution modes of both cases. That is, though the bending stress is far larger than the membrane stress in the case of a circular plate, the membrane stress is far larger than the bending stress for a cylindrical shell. Therefore, the strain hardening plastic range in the case of a plate appears on both surfaces for a small amount of load and the effect of hardening appears gradually. In the cylindrical shell, due to the large value of membrane stress, the stress distribution through the thickness is more uniform and the stress state through the thickness of the shell changes uniformly for larger value of pressure.

6(b). *Strain components*

As shown solid lines in Figs. 11 and 12, the relations between the axial strain components and the pressure at measuring points on the inner and outer surfaces are different from each other due to the effect of bending action and non-linearity of deformation. In order to grasp clearly such a complicated difference in these trends for the corresponding experiment, more measuring points of strain components were selected than in the case of

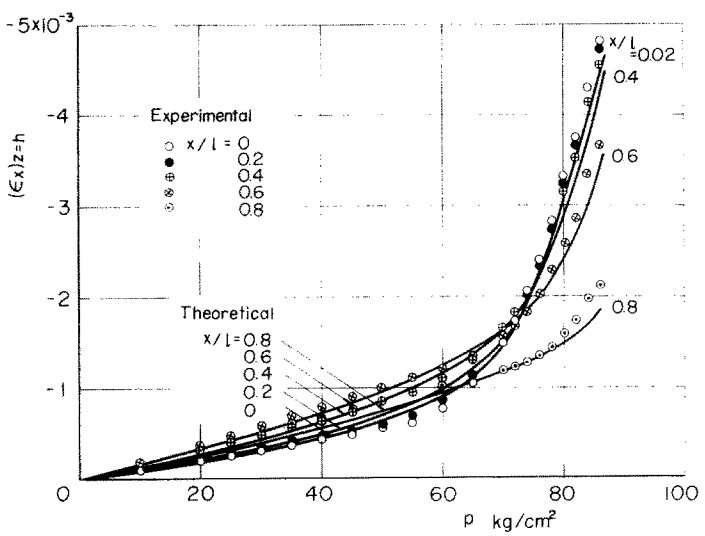

FIG. 11. Relation between axial strain component and pressure on inner ($z = h$) surface.

radial displacement. The solid curves in Fig. 13 show the relations between the circumferential strain component and pressure at the same points, and there is no difference on either surface from the assumption in the analysis. The various small circles show the experimental results at the measuring points, which are the mean values of strain distribution near the point on both surfaces, and they agree well with the corresponding analytical results.

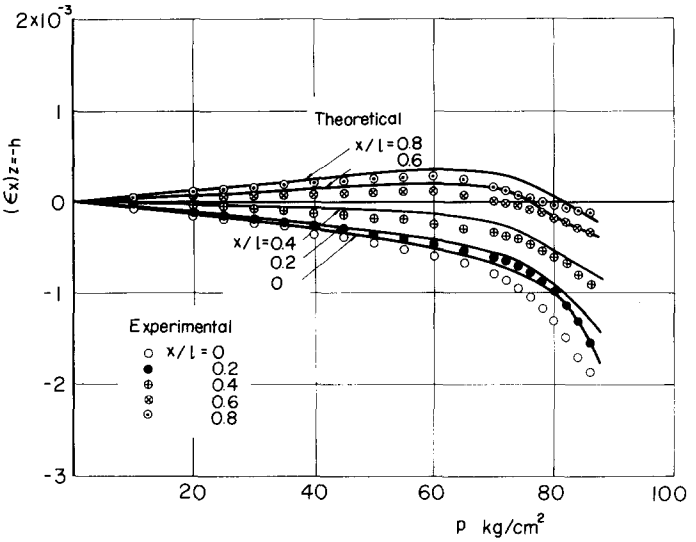

FIG. 12. Relation between axial strain component and pressure on outer ($z = -h$) surface.

In Fig. 11, though the sequence of absolute values of axial strain components on the inner surface $(\varepsilon_x)_{z=h}$ are $x/l = 0{\cdot}6, 0{\cdot}4, 0{\cdot}8, 0{\cdot}2$ and 0 in the range of $p \leq 57$ kg/cm^2, it varies thereafter and becomes as $x/l = 0, 0{\cdot}2, 0{\cdot}4, 0{\cdot}6$ and $0{\cdot}8$ for $p \geq 75$ kg/cm^2. This was corroborated very well by the corresponding experimental result as shown in Fig. 10.

In shell theory, assuming that the ratio $a/h = 40$ corresponds to a sufficiently thin shell, the result obtained by the membrane theory is applied. However, in the shorter cylindrical shell mentioned above, as shown in Figs. 11 and 12, it is confirmed clearly from the analytical and experimental results that large difference arises between the axial strain components on the outer and inner surfaces due to the effect of bending action.

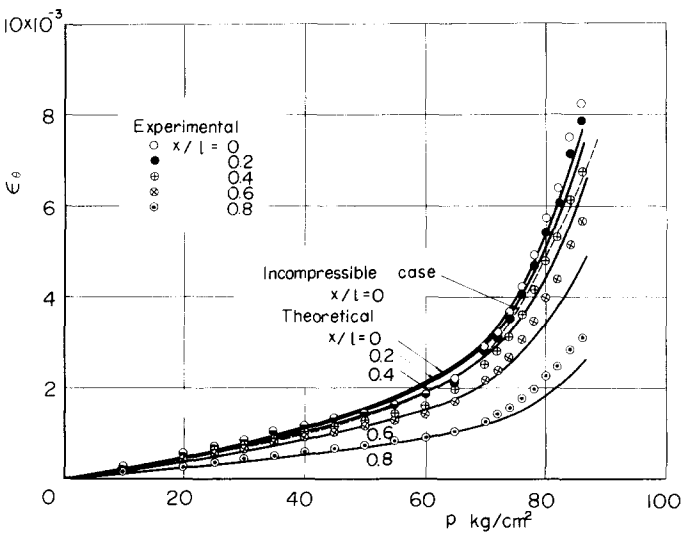

FIG. 13. Relation between circumferential strain component and pressure.

6(c). *Effect of compressibility of material to the analytical result*

In Fig. 13, the analytical result at $x/l = 0$, in which the material is assumed as incompressible, is also entered with a dashed line. As the value of w is very small and the errors arising from measurement and supported ends are apt to affect the experimental result, the comparison may be made more easily on the strain component ε_θ instead of w. Though the experimental value of ε_θ corresponds to the mean value in the range of 2 mm, as shown in Fig. 6, the strain distribution in this range may be considered as almost uniform. As shown in Fig. 13, the agreement between the experimental results and the solid curve is very good except where the dashed curve deviates to the lower side from the experimental results.

REFERENCES

[1] S. TIMOSHENKO and S. WOINOWSKY-KRIEGER, *Theory of Plates and Shells*, 2nd edition, p. 466. McGraw-Hill (1959).
[2] P. G. HODGE, JR., *Limit Analysis of Rotationally Symmetric Plates and Shells*, p. 52. Prentice-Hall (1963).
[3] W. OLSZAK and A. SAWCZUK, *Inelastic Behaviour in Shells*, p. 53. Noordhoff (1967).
[4] Y. OHASHI and N. KAMIYA, On the bending of thin plates of material having a non-linear stress–strain relation. *Int. J. Mech. Sci.* **9**, 183 (1967).
[5] Y. OHASHI and N. KAMIYA, Large deflection of a supported circular plate having a non-linear stress–strain relation. *Z. angew. Math. Mech.* **48**, 159 (1968).

APPENDIX

In the appendices, the following symbols are used for simplicity.

$S_0 = \sin\omega_0$, $C_0 = \cos\omega_0$, $S_1 = \sin\omega_1$, $C_1 = \cos\omega_1$, $C_{10} = \cos(\omega_1 - \omega_0)$, $S_{10} = \sin(\omega_1 - \omega_0)$,

$$\left.\begin{matrix} S_{p0} \\ S_{m0} \end{matrix}\right\} = \sin\left(\omega_0 \pm \frac{\pi}{3}\right), \qquad \left.\begin{matrix} C_{p0} \\ C_{m0} \end{matrix}\right\} = \cos\left(\omega_0 \pm \frac{\pi}{3}\right), \qquad \left.\begin{matrix} S_{p1} \\ S_{m1} \end{matrix}\right\} = \sin\left(\omega_1 \pm \frac{\pi}{3}\right)$$

$$\left.\begin{matrix} C_{p1} \\ C_{m1} \end{matrix}\right\} = \cos\left(\omega_1 \pm \frac{\pi}{3}\right),$$

$$L = \log[\{\beta + \cos(\omega_1 - \omega_0) + F_1\}/\{-\beta + \cos(\omega_1 - \omega_0) + F_{-1}\}],$$

$$\left.\begin{matrix} F_1^2 \\ F_{-1}^2 \end{matrix}\right\} = 1 \pm 2\beta\cos(\omega_1 - \omega_0) + \beta^2.$$

Appendix I

$$T_x = \tfrac{4}{3}h\left[2a_0E_1S_{p1} + \frac{1}{\sqrt{3}}a_1\frac{E_1^2}{\beta}\{\tfrac{2}{3}S_{p0}(F_1^3 - F_{-1}^3) + (S_{p1} - C_{10}S_{p0})(\beta(F_1 + F_{-1}) + C_{10}(F_1 - F_{-1}) + S_{10}^2L)\} + \tfrac{8}{3}a_2E_1^3\{\tfrac{1}{3}\beta^2(S_{p1} + 2C_{10}S_{p0}) + S_{p1}\} + \tfrac{32}{9}a_3E_1^5\{S_{p1}(1 + \tfrac{2}{3}\beta^2(1 + 2C_{10}^2) + \tfrac{1}{5}\beta^4) + 4\beta^2S_{p0}C_{10}(\tfrac{1}{3} + \tfrac{1}{5}\beta^2)\}\right],$$

$$M_x = \tfrac{4}{3}h^2E_1\left[\tfrac{2}{3}a_0\beta S_{p0}+\frac{1}{\sqrt{3}}a_1\frac{E_1}{\beta^2}\{\tfrac{1}{2}\beta S_{p0}(F_1^3+F_{-1}^3)+\tfrac{1}{3}(F_1^3-F_{-1}^3)(2S_{p1}-\tfrac{5}{2}S_{p0}C_{10})\right.$$
$$-(S_{p1}C_{10}-\tfrac{1}{4}S_{p0}(5C_{10}^2-1))(\beta(F_1+F_{-1})+C_{10}(F_1-F_{-1})+S_{10}^2L)\}+\tfrac{8}{3}a_2E_1^2\beta\{\tfrac{1}{5}\beta^2S_{p0}$$
$$\left.+\tfrac{1}{3}(S_{p0}+2S_{p1}C_{10})+\tfrac{32}{9}a_3E_1^4\beta\{4S_{p1}C_{10}(\tfrac{1}{3}+\tfrac{1}{5}\beta^2)+S_{p0}(\tfrac{1}{3}+\tfrac{2}{5}\beta^2(1+2C_{10}^2)+\tfrac{1}{7}\beta^4)\}\right].$$

The representations of T_θ and M_θ may be obtained by substituting $-S_{m0}$, $-C_{m0}$, $-S_{m1}$ and $-C_{m1}$ instead of S_{p0}, C_{p0}, S_{p1} and C_{p1} in the corresponding representations of T_x and M_x.

Appendix II

$$a_{11} = 2\left[a_0S_{p1}+\frac{1}{\sqrt{3}}a_1\frac{E_1}{\beta}\{\tfrac{2}{3}S_{p0}(F_1^3-F_{-1}^3)+(S_{p1}-S_{p0}C_{10})(\beta(F_1+F_{-1})+C_{10}(F_1-F_{-1})\right.$$
$$+S_{10}^2L)\}+4a_2E_1^2\{S_{p1}(\tfrac{1}{3}\beta^2+1)+\tfrac{2}{3}\beta^2S_{p0}C_{10}\}+\tfrac{80}{9}a_3E_1^4\{S_{p1}(1+\tfrac{2}{3}\beta^2(1+2C_{10}^2)+\tfrac{1}{5}\beta^4)$$
$$\left.+4\beta^2S_{p0}C_{10}(\tfrac{1}{3}+\tfrac{1}{5}\beta^2)\}\right],$$

$$a_{12} = E_1\left[-\frac{1}{\sqrt{3}}a_1\frac{E_1}{\beta^2}\{\tfrac{2}{3}S_{p0}(F_1^3-F_{-1}^3)+(S_{p1}-S_{p0}C_{10})(\beta(F_1+F_{-1})+C_{10}(F_1-F_{-1})+S_{10}^2L)\right.$$
$$-2\beta(S_{p0}(\beta(F_1-F_{-1})+C_{10}(F_1+F_{-1}))+(S_{p1}-S_{p0}C_{10})(F_1+F_{-1}))\}+\tfrac{16}{9}a_2E_1^2\beta(S_{p1}$$
$$\left.+2S_{p0}C_{10})+\tfrac{128}{9}a_3E_1^4\beta\{S_{p1}(\tfrac{1}{3}(1+2C_{10}^2)+\tfrac{1}{5}\beta^2)+2S_{p0}C_{10}(\tfrac{1}{3}+\tfrac{2}{5}\beta^2)\}\right],$$

$$a_{13} = E_1\left[2a_0C_{p1}+\frac{1}{\sqrt{3}}a_1\frac{E_1}{\beta}\{-2\beta S_{p0}S_{10}(F_1+F_{-1})+(C_{p1}S_{p0}S_{10})(\beta(F_1+F_{-1})\right.$$
$$+C_{10}(F_1-F_{-1})+S_{10}^2L)+2S_{10}(S_{p1}-S_{p0}C_{10})(C_{10}L-F_1+F_{-1})\}$$
$$+\tfrac{8}{3}a_2E_1^2\{(\tfrac{1}{3}\beta^2+1)C_{p1}-\tfrac{2}{3}\beta^2S_{p0}S_{10}\}+\tfrac{32}{9}a_3E_1^4\{C_{p1}(1+\tfrac{2}{3}\beta^2(1+2C_{10}^2)+\tfrac{1}{5}\beta^4)$$
$$\left.-4\beta^2S_{10}(\tfrac{2}{3}S_{p1}C_{10}+S_{p0}(\tfrac{1}{3}+\tfrac{1}{5}\beta^2))\}\right],$$

$$a_{21} = 2\left[\tfrac{1}{3}a_0\beta S_{p0}+\frac{1}{\sqrt{3}}a_1\frac{E_1}{\beta^2}\{\tfrac{1}{2}\beta S_{p0}(F_1^3+F_{-1}^3)+\tfrac{1}{3}(F_1^3-F_{-1}^3)(2S_{p1}-\tfrac{5}{2}S_{p0}C_{10})-(S_{p1}C_{10}\right.$$
$$-\tfrac{1}{4}S_{p0}(5C_{10}^2-1))(\beta(F_1+F_{-1})+C_{10}(F_1-F_{-1})+S_{10}^2L)\}+4a_2E_1^2\beta\{\tfrac{1}{5}\beta^2S_{p0}+\tfrac{1}{3}(S_{p0}$$
$$\left.+2S_{p1}C_{10})\}+\tfrac{80}{9}a_3E_1^4\beta\{4S_{p1}C_{10}(\tfrac{1}{3}+\tfrac{1}{5}\beta^2)+S_{p0}(\tfrac{1}{3}+\tfrac{2}{5}\beta^2(1+2C_{10}^2)+\tfrac{1}{7}\beta^4)\}\right],$$

$$a_{22} = E_1\left[\tfrac{2}{3}a_0S_{p0} - \frac{1}{\sqrt{3}}a_1\frac{E_1}{\beta^3}\{\tfrac{1}{2}\beta S_{p0}(F_1^3+F_{-1}^3) - \tfrac{3}{2}\beta^2 S_{p0}(\beta(F_1+F_{-1}) + C_{10}(F_1-F_{-1}))\right.$$
$$+(2S_{p1} - \tfrac{5}{2}S_{p0}C_{10})(\tfrac{2}{3}(F_1^3-F_{-1}^3) - \beta(\beta(F_1+F_{-1}) + C_{10}(F_1-F_{-1}))) + 2(\beta(F_1+F_{-1})$$
$$-\beta(F_1-F_{-1}) + C_{10}(F_1+F_{-1}) + S_{10}^2L))(S_{p1} - \tfrac{1}{4}S_{p0}(5C_{10}^2-1))\} + \tfrac{8}{3}a_2E_1^2\{\tfrac{3}{5}\beta^2S_{p0}$$
$$\left.+\tfrac{1}{3}(S_{p0}+2S_{p1}C_{10})\} + \tfrac{32}{9}a_3E_1^4\{4S_{p1}C_{10}(\tfrac{1}{3}+\tfrac{3}{5}\beta^2) + S_{p0}(\tfrac{1}{3}+\tfrac{6}{5}\beta^2(1+2C_{10}^2) + \tfrac{5}{7}\beta^4)\}\right],$$

$$a_{23} = E_1\left[\frac{1}{\sqrt{3}}a_1\frac{E_1}{\beta^2}\{-\tfrac{3}{2}\beta^2S_{p0}S_{10}(F_1-F_{-1}) - \beta S_{10}(F_1+F_{-1})(2S_{p1} - \tfrac{5}{2}S_{p0}C_{10})\right.$$
$$+\tfrac{1}{3}(F_1^3-F_{-1}^3)(2C_{p1} + \tfrac{5}{2}S_{p0}S_{10}) - 2S_{10}(C_{10}L - F_1 + F_{-1})(S_{p1}C_{10} - \tfrac{1}{4}S_{p0}(5C_{10}^2-1))$$
$$\left.-(C_{p1}C_{10} - S_{p1}S_{10} + \tfrac{5}{2}S_{p0}C_{10}S_{10})\} + \tfrac{16}{9}a_2E_1^2\beta(C_{p1}C_{10} - S_{p1}S_{10})\right.$$
$$\left.+\tfrac{128}{9}a_3E_1^4\beta\{(\tfrac{1}{3}+\tfrac{1}{5}\beta^2)(C_{p1}C_{10} - S_{p1}S_{10}) - \tfrac{2}{5}\beta^2S_{p0}S_{10}C_{10}\}\right],$$

$$a_{31} = C_{p1} + cC_1, \qquad a_{32} = 0, \qquad a_{33} = -E_1(S_{p1} + cS_1),$$

$$b_1 = 0, \qquad b_2 = \tfrac{3}{4}Q_x/h(l/h), \qquad b_3 = \tfrac{3}{2}s(l/a).$$

Appendix III

As the representations shown in Appendices I and II are unavailable at $\beta = 0$, it is necessary to find the limit of their values for $\beta \to 0$. Only the limit values different from those shown in Appendices I and II are shown in the following.

$$T_x = \tfrac{8}{3}E_1hS_{p1}\left(a_0 + \frac{2}{\sqrt{3}}a_1E_1 + \tfrac{4}{3}a_2E_1^2 + \tfrac{16}{9}a_3E_1^4\right),$$

$$T_\theta = -\tfrac{8}{3}E_1hS_{m1}\left(a_0 + \frac{2}{\sqrt{3}}a_1E_1 + \tfrac{4}{3}a_2E_1^2 + \tfrac{16}{9}a_3E_1^4\right),$$

$$M_x = M_\theta = 0,$$

$$a_{11} = 2S_{p1}\left(a_0 + \frac{4}{\sqrt{3}}a_1E_1 + 4a_2E_1^2 + \tfrac{80}{9}a_3E_1^4\right), \qquad a_{12} = 0,$$

$$a_{13} = 2E_1C_{p1}\left(a_0 + \frac{2}{\sqrt{3}}a_1E_1 + \tfrac{4}{3}a_2E_1^2 + \tfrac{16}{9}a_3E_1^4\right), \qquad a_{21} = 0,$$

$$a_{22} = \tfrac{2}{3}E_1S_{p0}\left(a_0 + \frac{2}{\sqrt{3}}a_1E_1 + \tfrac{4}{3}a_2E_1^2 + \tfrac{16}{9}a_3E_1^4\right) + \tfrac{4}{3}E_1S_{p1}C_{10}\left(\frac{1}{\sqrt{3}}a_1E_1 + \tfrac{4}{3}a_2E_1^2 + \tfrac{32}{9}a_3E_1^4\right),$$

$$a_{23} = 0.$$

(*Received* 28 *February* 1969; *revised* 8 *September* 1969)

Абстракт—С целью анализа деформации, вызванной внутренним давлением, тонких цилиндрических оболочек из материалов обладающих нелинейными зависимостями напряжение-деформация, определяются основные уравнения, используя гипотезу Кирхгоффа и вводя параметр, указывающий эффект сжимаемости материала. Уравнения применяются для случая опертой короткой цилиндрической оболочки из алюминиего сплава, под внутренным давлением. Для исследования важности предположений, сравниваются аналитические результаты с экспериментальными.

Аналитические результаты компонентов осевой деформации разнятся значительно на внешней и внутренней поверхностях. Сложное изменение распределения осевой деформации на внутренной поверхности при росте давления приписывается нелинейности деформации. Такое направление сравнивается ясно путем соответствующего эксперимента.